Inorganic Chemistry
Communication

Inorg. Chem. **2010**, *49*, 8179–8181 **8179**
DOI: 10.1021/ic100719r

Application of High Surface Area Tin-Doped Indium Oxide Nanoparticle Films as Transparent Conducting Electrodes

Paul G. Hoertz,† Zuofeng Chen, Caleb A. Kent, and Thomas J. Meyer*

Department of Chemistry, University of North Carolina at Chapel Hill, Chapel Hill, North Carolina 27599.
†Current Address: RTI International, Center for Aerosol Technology, Research Triangle Park, North Carolina 27709.

Received April 14, 2010

Metal complex derivatized, optically transparent nanoparticle films of Sn(IV)-doped In_2O_3 (*nano*ITO) undergo facile interfacial electron transfer allowing for rapid, potential controlled color changes, direct spectral (rather than current) monitoring of voltammograms, and multilayer catalysis of water oxidation.

Surface-derivatized, semiconducting nanoparticles in thin porous films are a hallmark of dye-sensitized solar cells (DSSCs), first reported by Grätzel and O'Regan in 1991.[1] They are transparent in the visible with effective surface areas that can be thousands of times greater than those of planar electrodes. Their high porosities allow for internal diffusion of solvent and electrolytes.[2,3] A conductive, high surface area equivalent with broad spectral transparency could have considerable value in a variety of applications. Conductive, porous nanoparticle films of metals such as Au have been reported but are highly absorbing, even at thicknesses < 100 nm.[4] Transparent, partly conductive Sb-doped SnO_2 nanoparticle and mesoporous films have been reported and applied in electrochromic and electrochemiluminescent devices.[5−7] Reports of conductive, porous films of Sn(IV)-doped In_2O_3 (*nano*ITO) have also appeared but without application of surface derivatization and optical-electrochemical monitoring.[8−14] A template-directed, sol−gel preparation of mesoporous ITO with a redox active, surface-bound silane ferrocene derivative has been reported,[10] and ITO nanoparticle films have been used as an electrical conduit for reversible oxidation/reduction of deposited Prussian Blue.[8]

We report here the preparation and characterization of optically transparent *nano*ITO films derivatized with surface-bound chromophores and molecular catalysts at levels comparable to those of *nano*TiO_2. In contrast to *nano*TiO_2, surface derivatives on *nano*ITO undergo facile interfacial electron transfer allowing for rapid, reversible, potential controlled color changes, direct spectral (rather than current) monitoring of voltammograms, and multilayer catalysis of water oxidation.

*Nano*ITO films were prepared by spin-coating a suspension of ∼40 nm ITO nanoparticles onto planar substrates (e.g., borosilicate glass, fused silica, FTO (fluoride-doped SnO_2), or ITO). Once formed, films were annealed in the air at 500 °C for 1 h and then at 300 °C under 3% H_2/N_2 for an additional hour (Table S1, Supporting Information). Thickness was controlled by varying nanoparticle concentration in the suspension: 0.55 μm for 12 wt %, 2.5 μm for 22 wt %, 6.7 μm for 29 wt %, and 15.7 μm for 36 wt %, Figure S1 (Supporting Information). Top-down and cross-sectional field emission scanning electron microscope (FESEM) images demonstrate that the films are highly porous and uniform, allowing for the diffusion of the solvent and electrolyte within the porous film structure, Figure 1.

The resistance across 1 cm of a 0.55-μm-thick film, annealed in the air on glass, by two-point probe measurements was 31 kΩ, and 1.7 kΩ for a 15.7-μm-thick film. Hydrogen annealing decreased the resistance to 840 Ω and 50 Ω, respectively (Table S2, Supporting Information). A four-point probe measurement on the latter film gave 45 Ω

*To whom correspondence should be addressed. E-mail: tjmeyer@unc.edu.

(1) O'Regan, B.; Gratzel, M. *Nature* **1991**, *353*, 737–740.
(2) Gratzel, M. *Inorg. Chem.* **2005**, *44*, 6841–6851.
(3) Meyer, G. J. *Inorg. Chem.* **2005**, *44*, 6852–6864.
(4) Ding, Y.; Chen, M. *MRS Bull.* **2009**, *34*, 569–576.
(5) Schwab, P. F. H.; Diegoli, S.; Biancardo, M.; Bignozzi, C. A. *Inorg. Chem.* **2003**, *42*, 6613–6615.
(6) Biancardoa, M.; Argazzi, R.; Bignozzi, C. A. *Displays* **2006**, *27*, 19–23.
(7) Hou, K.; Puzzo, D.; Helander, M. G.; Lo, S. S.; Bonifacio, L. D.; Wang, W.; Lu, Z.-H.; Scholes, G. D.; Ozin, G. A. *Adv. Mater.* **2009**, *21*, 2492–2496.
(8) Cheng, K.-C.; Chen, F.-R.; Kai, J.-J. *Electrochim. Acta* **2007**, *52*, 3330–3335.
(9) Ederth, J.; Hultaker, A.; Niklasson, G. A.; Heszler, P.; van Doorn, A. R.; Jongerius, M. J.; Burgard, D.; Granqvist, C. G. *Appl. Phys. A: Mater. Sci. Process.* **2005**, *81*, 1363–1368.
(10) Fattakhova-Rohlfing, D.; Brezesinski, T.; Rathouský, J.; Feldhoff, A.; Oekermann, T.; Wark, M.; Smarsly, B. *Adv. Mater.* **2006**, *18*, 2980–2983.
(11) Goebbert, C.; Nonningerb, R.; Aegerter, M. A.; Schmidt, H. *Thin Solid Films* **1999**, *351*, 79–84.
(12) Gross, M.; Winnacker, A.; Wellmann, P. J. *Thin Solid Films* **2007**, *515*.
(13) Lin, H.; Jin, T.; Dmytruk, A.; Saito, M.; Yazawa, T. *J. Photochem. Photobiol., A* **2004**, *164*, 173–177.
(14) Puetz, J.; Al-Dahoudi, N.; Aegarter, M. A. *Adv. Eng. Mater.* **2004**, *6*, 733.

Published on Web 08/16/2010

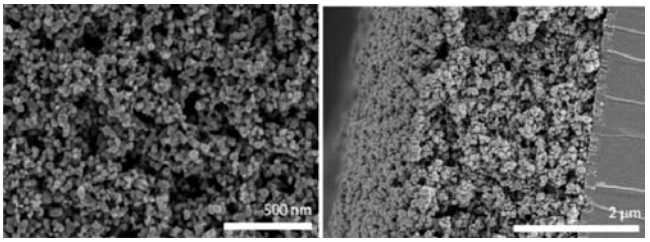

Figure 1. Top-down (left) and cross-sectional (right) field emission scanning electron microscopy (FESEM) images of an ITO|*nano*ITO slide (2.5 μm) annealed in the air at 500 °C and under a steady flow of 3% H_2/N_2 at 300 °C. For both images, a thin coating of Au/Pd was deposited prior to imaging.

over an applied potential range of ±1 V. The effects of various annealing conditions are summarized in Table S3 (Supporting Information).

UV−visible−near IR measurements on dry *nano*ITO films, Figure S2 (Supporting Information), show that underivatized films are largely transparent above 400 nm with an apparent near-UV absorption that tails into the visible spectrum. This feature increases with film thickness and is attributable to light scattering by nanoparticle aggregates.[15] Hydrogen annealed films have a bluish cast, while films annealed under atmospheric conditions have a light yellow cast.

After exposing a *nano*ITO film on ITO (ITO|*nano*ITO) to a 0.1 mM methanolic solution of the phosphonate derivative salt, $[Ru(bpy)_2(4,4'\text{-}PO_3H_2\text{-}bpy)](PF_6)_2$ (4,4′-PO_3H_2-bpy is 4,4′-diphosphonato-2,2′-bipyridine), a characteristic metal-to-ligand charge transfer (MLCT) absorption band appears at λ_{max} = 453 nm, Figure S3 (Supporting Information). Complete surface coverages ($\Gamma_o \sim 2.5 \times 10^{-8}$ mol/cm^2) were reached within 3 h for 2.5 μm film thicknesses. Surface coverages were estimated from the relationship $\Gamma = A(\lambda)/(10^3 \times \varepsilon(\lambda))$, with $A(\lambda)$ the absorbance at λ and $\varepsilon(\lambda) = \varepsilon_{max} = 9.0 \times 10^3$ M^{-1}cm^{-1} for $[Ru(bpy)_2(4,4'\text{-}PO_3H_2\text{-}bpy)]^{2+}$ in methanol at 453 nm.[16] On the basis of Langmuir isotherm measurements, Figure S4 (Supporting Information), $K = 1.4 \times 10^5$ M^{-1} for surface binding in methanol at 25 °C, as determined by spectrophotometric measurements and the relationship, $\Gamma = \Gamma_o[M]/([M] + 1/K)$. In this equation, Γ_o is the coverage for a fully loaded surface and Γ is the equilibrium coverage at molar concentration [M].[17]

Adsorbed $[Ru(bpy)_2(4,4'\text{-}PO_3H_2\text{-}bpy)]^{2+}$ in films of *nano*ITO on conducting ITO, ITO|*nano*ITO-Ru^{II}, is relatively stable on the surface. On the basis of UV−visible measurements, there was no loss of complex after soaking in 0.1 M $HClO_4$ for 15 h, while 10% of the complex was lost after 4 days in neutral, deionized water. As expected, surface coverages increase linearly with film thickness, from 5.5×10^{-9} mol/cm^2 (0.55 μm) to 1.6×10^{-7} mol/cm^2 (15.7 μm). At 0.55 μm, the effective sensitizer surface coverage is ~34 times greater than for planar FTO or ITO electrodes (~1.6×10^{-10} mol/cm^2), increasing to ~1000 times for 15.7 μm films.

Figure 2 shows cyclic voltammograms (CVs) for ITO|*nano*ITO-Ru^{II} and background scans in water and acetonitrile (MeCN). A fully reversible wave is observed for the

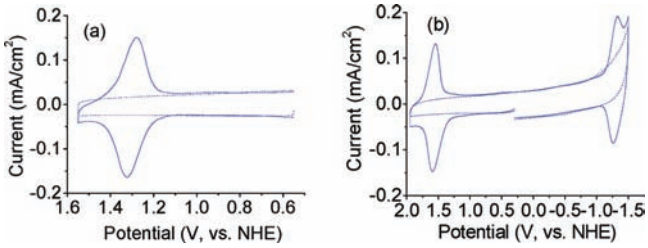

Figure 2. Cyclic voltammograms (CVs) of ITO|*nano*ITO-Ru(bpy)$_2$(4,4′-PO_3H_2-bpy)]$^{2+}$(ITO|*nano*ITO-Ru^{II}): (a) in aqueous 0.1 M $HClO_4$ or (b) in 0.1 M ^{n}Bu$_4$NPF$_6$/MeCN (deaerated). Thickness, 2.5 μm; scan rate, 10 mV/s. The dotted lines are ITO|*nano*ITO backgrounds.

surface-bound Ru$^{III/II}$ couple, $E_{1/2}$(Ru$^{III/II}$) = 1.3 V vs NHE in 0.1 M $HClO_4/H_2O$, Figure 2a. As shown in Figure 2b, in 0.1 M ^{n}Bu$_4$NPF$_6$/MeCN, the Ru$^{III/II}$ couple appears at 1.57 V and a reversible ITO|*nano*ITO-Ru^{II}(bpy)$^{2+}$/Ru^{II}(bpy$^-$)$^+$ reduction wave at $E_{1/2}$ = −1.26 V vs NHE. As shown in Figure S5 (Supporting Information), there is an extended reductive background compared to *nano*TiO_2. For background subtracted CVs of ITO|*nano*ITO-Ru^{II}, peak currents (i_p) for the Ru$^{III/II}$ couple vary linearly with the scan rate at low scan rates (≤50 mV/s) for thicknesses from 0.55 to 2.5 μm in both solvents, and peak-to-peak splittings ($\Delta E_p = E_{p,a} - E_{p,c}$) are less than 50 mV. These results are consistent with kinetically facile electron transfer to and from surface-confined redox couples, Figure S6 (Supporting Information). At higher scan rates, the peak-to-peak splitting increases with both the scan rate and thickness, Figure S7 (Supporting Information).

Current densities greatly exceed those for the same complex on planar ITO or FTO electrodes. A current density of 125 μA/cm^2 (background subtracted) for a 2.5 μm *nano*ITO-Ru^{II} film was observed compared to 0.9 μA/cm^2 for planar ITO at a scan rate of 10 mV/s. This gives a surface roughness factor of 140 relative to planar surfaces. A comparison of surface coverages from UV−visible and CV peak current measurements shows that ~90% of the adsorbed Ru^{II} sites in *nano*ITO-Ru^{II} are oxidized during an oxidative excursion from 0.55 to 1.5 V at 10 mV/s.

The scan rate dependence of background, non-Faradaic currents at 1.3 V were measured for underivatized films in 0.1 M $HClO_4/H_2O$ and 0.1 M ^{n}Bu$_4$NPF$_6$/MeCN, Figure S8 (Supporting Information). A linear relationship was observed between double-layer charging current and the scan rate at scan rates > 50 mV/s in 0.1 M ^{n}Bu$_4$NPF$_6$/MeCN, with slopes increasing from 0.5 mA·s/cm^2·mV for 0.55-μm-thick films to 5 mA·s/cm^2·mV at 15.7 μm, consistent with well-defined capacitive behavior.

Spectroelectrochemical measurements on ITO|*nano*ITO-Ru^{II} demonstrate reversibility through multiple oxidative, ITO|*nano*ITO-Ru$^{III/II}$, and reductive, -Ru$^{2+/+}$, cycles. As shown in Figure 3a, in aqueous 0.1 M $HClO_4$, this enables direct spectral (rather than current) monitoring of ITO|*nano*ITO-Ru$^{III/II}$ voltammograms during an oxidative excursion from 0.55 to 1.55 V at 10 mV/s. Oxidation results in the quantitative conversion of *nano*ITO-Ru^{II} (λ_{max} = 453 nm) to *nano*ITO-Ru^{III} ($\lambda_{max} \sim 650$ nm) and, as shown in the inset, is quantitatively reversible. Similarly, a reductive excursion through the *nano*ITO-Ru$^{2+/+}$ wave in deaerated 0.1 M ^{n}Bu$_4$NPF$_6$/MeCN results in reversible reduction to *nano*ITO-Ru(bpy$^-$)(bpy)$_2^+$ (λ_{max} = 494 nm).

(15) Barbé, C. J.; Arendse, F.; Comte, P.; Jirousek, M.; Lenzmann, F.; Shklover, V.; Grätzel, M. *J. Am. Ceram. Soc.* **1997**, *80*, 3157–71.
(16) Gillaizeau-Gauthier, I.; Odobel, F.; Alebbi, M.; Argazzi, R.; Costa, E.; Bignozzi, C. A.; Qu, P.; Meyer, G. J. *Inorg. Chem.* **2001**, *40*, 6073–6079.
(17) Galoppini, E.; Guo, W.; Zhang, W.; Hoertz, P. G.; Qu, P.; Meyer, G. J. *J. Am. Chem. Soc.* **2002**, *124*, 7801–7811.

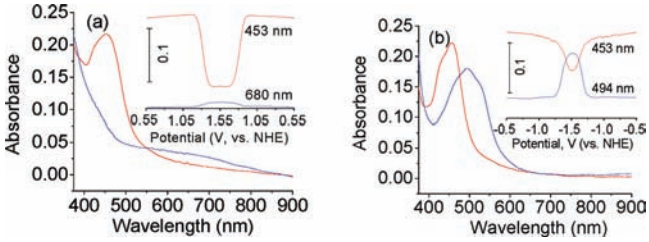

Figure 3. (a) UV−visible spectra of ITO|*nano*ITO-Ru^{II} (2.5 μm) at an applied potential of 0.55 V vs NHE (red line) and at 1.55 V (blue line) in 0.1 M $HClO_4$ during a CV scan at 10 mV/s. The inset shows potential-dependent changes at 453 and 680 nm during the optically monitored voltammogram for both oxidative and reductive scans. (b) As in (a), in deaerated 0.1 M $^nBu_4NPF_6$/MeCN for reduction from −0.5 V (ITO|*nano*ITO-$Ru^{II}(bpy)^{2+}$, red line) to −1.5 V (ITO|*nano*ITO-$Ru^{II}(bpy^{\bullet-})^{+}$, blue line). The inset shows the time-dependent changes at 453 and 494 nm during the voltammogram.

For a potential step from 0.55 to 1.45 V vs NHE, well past $E^{\circ\prime}$ for the *nano*ITO-$Ru^{III/II}$ couple, oxidation was complete in <2 s in a film of thickness 2.5 μm, Figure S9 (Supporting Information). Stepping the potential from 1.45 to 0.55 V results in complete recovery of the original Ru^{II} spectrum. The $Ru^{III/II}$ redox cycle was repeated 360 times without significant change, Figure S10 (Supporting Information). There is no luminescence from *nano*ITO-Ru^{II} consistent with the conducting nature of *nano*ITO as the substrate, Figure S11.

Earlier, we reported water oxidation catalysis by the single-site, surface-bound catalyst $[Ru(Mebimpy)(4,4'\text{-}((HO)_2OP\text{-}CH_2)_2bpy)(OH_2)]^{2+}$ (**1-PO_3H_2**) (Mebimpy is 2,6-bis(1-methylbenzimidazol-2-yl)pyridine) on ITO, FTO, and FTO|*nano*TiO_2 electrodes.[18] The catalyst complex adsorbs to *nano*ITO with a surface binding constant of $K = 9 \times 10^4\ M^{-1}$. In cyclic voltammograms at pH 1 (0.1 M HNO_3), Figure S12 (Supporting Information), surface waves appear for the $Ru-OH_2^{3+}/Ru^{II}-OH_2^{2+}$, $Ru^{IV}=O^{2+}/Ru^{III}-OH_2^{2+}$, and $Ru^{V}=O^{3+}/Ru^{IV}=O^{2+}$ couples at $E_{1/2} = 0.81$, 1.25, and 1.60 V vs NHE, respectively, and the surface peroxide couples $Ru^{III}-OOH^{2+}/Ru^{II}(HOOH)^{2+}$ and $Ru^{IV}(OO)^{2+}/Ru^{III}-OOH^{2+}$ at $E_{1/2} =$ 0.42 and 0.52 V. The latter are observed following an oxidative scan past the $Ru^{V}=O^{3+}/Ru^{IV}=O^{2+}$ couple.[18]

(18) Chen, Z. F.; Concepcion, J. J.; Jurss, J. W.; Meyer, T. J. *J. Am. Chem. Soc.* **2009**, *131*, 15580–15581.

The surface-bound complex on *nano*ITO, ITO|*nano*ITO-**1-PO_3H_2**, is also an effective electrocatalyst for water oxidation. Following a potential step to 1.85 V at pH 5 ($I =$ 0.1 M, CH_3CO_2H/CH_3CO_2Na), sustained catalytic currents are observed with a turnover rate, $i_{cat}/nFA\Gamma$, of $\sim$0.027 s^{-1}. In this expression, i_{cat} is the catalytic current, n the number of electrons transferred per redox event (4 e^-), and A the surface area in cm^2. The catalytic current density observed for 2.5 μm ITO|*nano*ITO-**1-PO_3H_2** constitutes an 11-fold enhancement relative to ITO-**1-PO_3H_2** and a 12-fold/μm improvement relative to ITO|*nano*TiO_2-**1-PO_3H_2**.[18] On *nano*ITO, electrocatalytic activity was maintained for at least 8 h corresponding to $\sim$800 turnovers per catalyst site.

The *nano*ITO films described here combine high surface area, optical transparency, and high electrical conductivity. They provide a basis for optical monitoring of voltammograms and electrocatalysis and are of value in mechanistic studies by real time spectroscopic measurement of electrochemical reactions and intermediates. The wide potential window and relatively rapid electron transfer characteristics also point to possible electrochromic, display, and photovoltaic applications.

Acknowledgment. Initial funding by the Chemical Sciences, Geosciences and Biosciences Division of the Office of Basic Energy Sciences, U.S. Department of Energy, through Grant DE-FG02-06ER15788, Army Research Office through Grant W911NF-09-1-0426 for surface measurements (Z.C.), and the UNC EFRC: Solar Fuels and Next Generation Photovoltaics, an Energy Frontier Research Center also funded by U.S. DOE-BES, under Award DE-SC0001011 (P.G.H. and C.A.K.) is gratefully acknowledged.

Supporting Information Available: Experimental procedures and information, heating programs, resistance data, a plot of film thickness by concentration, UV−vis spectra, adsorption isoterms, CVs, a plot of the dependence of the peak current of the Ru(III/II) redox couple on the scan rate, plots of changes in absorbance with time, and photoluminescence data. This material is available free of charge via the Internet at http://pubs.acs.org.